Journal of Structural Geology 33 (2011) 132–144

Contents lists available at ScienceDirect

Journal of Structural Geology

journal homepage: www.elsevier.com/locate/jsg

Fault rocks from the SAFOD core samples: Implications for weakening at shallow depths along the San Andreas Fault, California

R.E. Holdsworth [a,*], E.W.E. van Diggelen [b], C.J. Spiers [b], J.H.P. de Bresser [b], R.J. Walker [a], L. Bowen [a,c]

[a] Reactivation Research Group, Department of Earth Sciences, University of Durham, Durham DH1 3LE, UK
[b] HPT Laboratory, Utrecht University, Utrecht, The Netherlands
[c] Durham GJ Russell Microscopy Facility, Durham University, Durham DH1 3LE, UK

ARTICLE INFO

Article history:
Received 9 September 2010
Received in revised form
11 November 2010
Accepted 18 November 2010
Available online 3 December 2010

Keywords:
San Andreas Fault
SAFOD
Fault zone weakening
Smectite
Phyllosilicate
Fluid-assisted alteration

ABSTRACT

The drilling of a deep borehole across the actively creeping Parkfield segment of the San Andreas Fault Zone (SAFZ), California, and collection of core materials permit direct geological study of fault zone processes at 2–3 km depth. The three drill cores sample both host and fault rocks and pass through two currently active, narrow (1–2 m wide) shear zones enclosed within a broader (ca. 240 m wide) region of inactive foliated gouges. The host rocks preserve primary sedimentary features and are cut by numerous minor faults and small, mainly calcite-filled veins. The development of Fe-enriched smectitic phyllosilicate networks following cataclasis is prevalent in the presently inactive foliated gouges of the main fault zone and in minor faults cutting clay-rich host rocks. Calcite, anhydrite and minor smectitic phyllosilicate veins are interpreted to have formed due to local fluid overpressuring events prior to, synchronous with and after local gouge development. By contrast, the active shear zone gouges lack mineral veins (except as clasts) and contain numerous clasts of serpentinite. Markedly Mg-rich smectitic phyllosilicates are the dominant mineral phases here, suggesting that the fault zone fluids have interacted with the entrained serpentinites. We propose that weakening of the SAFZ down to depths of at least 3 km can be attributed to the pervasive development of interconnected networks of low friction smectitic phyllosilicates and to the operation of stress-induced solution-precipitation creep mechanisms.

1. Introduction

Most geological faults are likely to be weak in a relative sense compared to nearby regions of intact host rock. However, geophysical measurements of surface heat flow (e.g. Brune et al., 1969; Lachenbruch and Sass, 1980) and stress orientation data (Mount and Suppe, 1987; Zoback et al., 1987) adjacent to crustal-scale faults, especially those sections of such faults undergoing creep, have demonstrated the existence of anomalously low frictional strengths, i.e. they are weak in an absolute sense, with friction coefficients (μ) significantly less than 0.6. The causes, global importance and very existence of such anomalous weakness along faults remain highly controversial issues despite over forty years of research (e.g. see Scholz, 2000; Zoback, 2000). The recent deep drilling into an active segment of the San Andreas Fault Zone (SAFZ) at seismogenic depths (Zoback et al., 2007, 2010) provides an opportunity to directly sample and study core materials to assess the mineralogy, deformation mechanisms and laboratory-measured constitutive properties of fault rocks. Unlike fault rocks in surface exposures, materials recovered from such in-situ sampling at depth have not experienced recent surface alteration. This means that they potentially preserve a more accurate record of deformation and associated mineralogical changes that occur during faulting.

The present paper outlines a geological description and interpretation of the lithologies, meso- and micro-structures found in the three sections of core from the San Andreas Fault Observatory at Depth (SAFOD) (Fig. 1). Unlike most studies published to date, which have focussed on isolated samples, the findings presented here are based on a visual assessment of *all* Phase 3 core materials, and on detailed optical microscope- and SEM-based studies of 38 representative thin sections taken from those cores. These include all of the thin sections prepared for the Phase 3 core atlas (SAFOD, 2010). The observations made using the SEM are supplemented by use of Energy Dispersive X-ray (EDX) analyses to identify specific mineral grains and produce elemental maps of selected regions. The overview presented here is intended to provide some important preliminary geological constraints for many of the more detailed studies being carried

* Corresponding author. Tel.: +44 0 1913342299; fax: +44 0 1913342301.
E-mail address: r.e.holdsworth@durham.ac.uk (R.E. Holdsworth).

0191-8141/$ – see front matter © 2010 Elsevier Ltd. All rights reserved.
doi:10.1016/j.jsg.2010.11.010

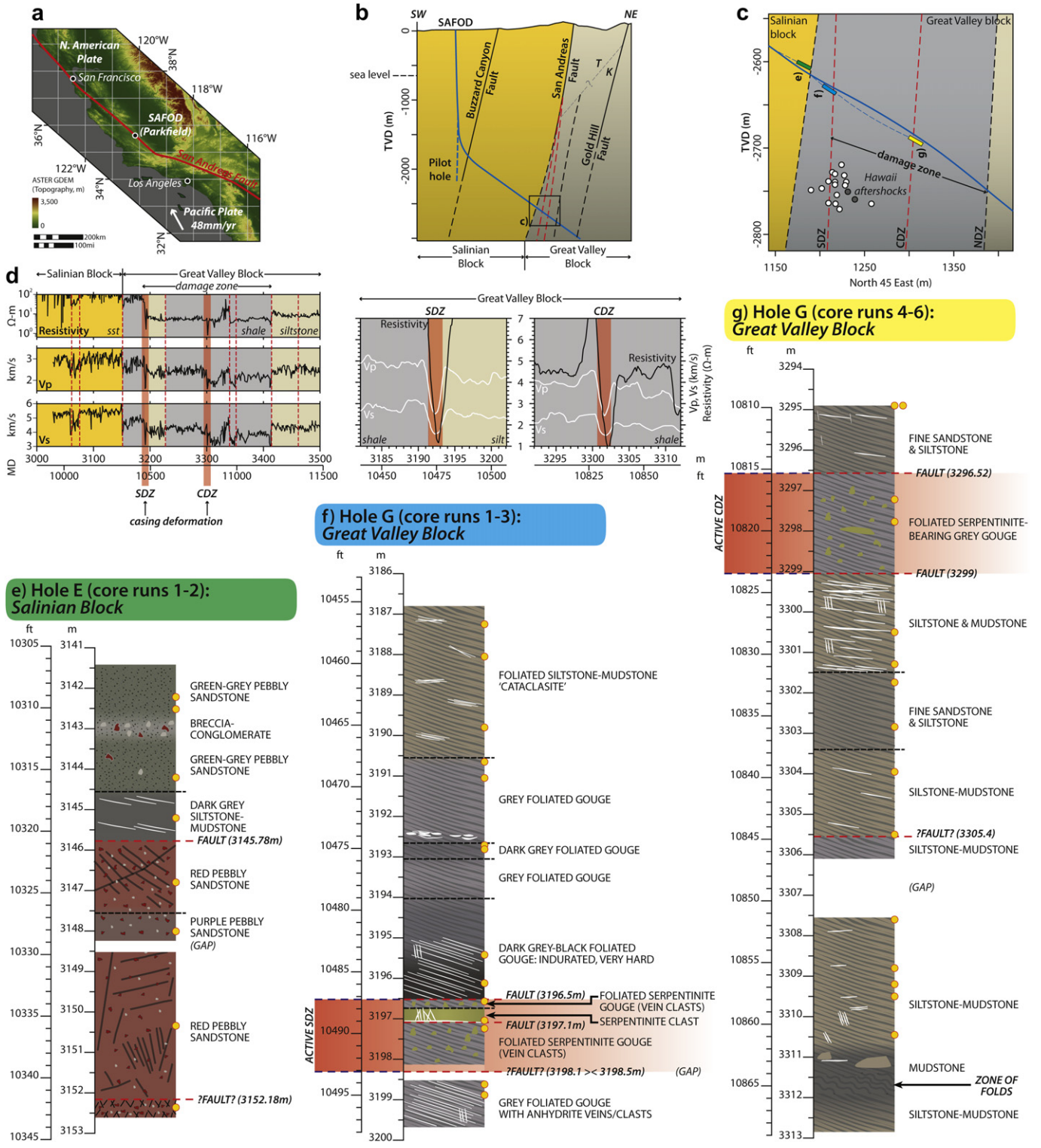

Fig. 1. a) General location map of the SAFZ and SAFOD borehole, Parkfield, California. Topography based on the ASTER GDEM. (b) Highly simplified NW-SE cross-section showing steep SW dip of SAFZ and its bifurcation into at least 3 strands at depth, at least 2 of which (shown in red) are actively creeping. Box shows location of (c). (c) Cross-section showing inclined borehole crossing SAFZ and approximate location of Phase 3 cores. These are colour-coded to the logs shown in Fig. 1e–g. (d) Left-hand image shows simplified geophysical logs and geology with depth along the Phase 2 borehole (after Zoback et al., 2010). Dashed red lines represent faults, whilst thick red zones correspond to the SDZ and CDZ where active creep has deformed the borehole casing. The broader damage zone is also shown corresponding to the region of lower resistivity and seismic velocities. Right-hand images show detail of the geophysical log properties in the region of the SDZ (left) and CDZ (right). The measured depths shown are for the Phase 2 borehole (see note below). (e)–(g) Simplified geological logs of the Phase 3 cores based on the descriptions given in the Core Atlas (SAFOD 2010) together with a preliminary visual inspection of the core (in 2007) and a more detailed visual inspection using the On-line Core Viewer (http://www.earthscope.org/data/safod_core_viewer). Important note: The measured depths shown here are for the Phase 3 drilling, but the cores here were drilled as a series of multilaterals off the Phase 2 hole. As a result, the measured depths do not necessarily coincide. However, Zoback et al. (2010) have shown that the markedly anomalous geophysical signatures of the active SDZ and CDZ allow a synchronization of measured depths for the two sets of core runs taken from Hole G. Thus it is suggested that in core runs 1–3 (SDZ), 5.03 m should be *subtracted* from the Phase 3 m Md values to synchronise them with the Phase 2 values, whilst 3.96 m should be *added* to the Phase 3 m Md values in core runs 4–6 (CDZ). Locations of thin sections examined during the present study are shown as yellow dots.

out by other geoscientists focussed on individual samples and short sections of the core material.

2. SAFOD: geological setting and location of borehole

The San Andreas Fault forms the steeply dipping to sub-vertical dextral transcurrent boundary between the Pacific plate to the west and the North American plate to the east (Fig. 1a and b). The fault zone is over 1000 km long, extends at depth to at least 15 km, and is manifested at the surface by a complex zone of linked faults and associated brittle deformation ranging from a few hundred metres to several kilometres wide (Allen, 1981). Geophysical data have repeatedly demonstrated that the direction of maximum horizontal stress in the crust lies at a high angle to the San Andreas Fault tract throughout central California and remains at a high angle to within 200 m of the active fault traces within the SAFOD boreholes (e.g. Hickman and Zoback, 2004; Zoback and Hickman, 2005; Boness and Zoback, 2006). This evidence, together with the absence of any measureable heat flow anomaly, either regionally or in any of the SAFOD boreholes (e.g. Sass et al., 1997; Williams et al., 2005) strongly suggests that active creep (at ~2.5 cm/year; Titus et al., 2006) along the Parkfield segment of the San Andreas Fault (Fig. 1a) occurs at very low values of resolved shear stress. Following the drilling of the main SAFOD borehole, it became apparent that two narrow (1–2 m wide) sections were undergoing active deformation by creep due to localised fault movements at 3192 m and 3302 m Md (= Measured depth, in this case along the length of the Phase 2 borehole). Following Zoback et al. (2010), these active regions are referred to here as the *southwest deforming zone* (SDZ) and the *central deforming zone* (CDZ) (Fig. 1b and c). During the final stage of drilling, Phase 3, a series of multilaterals were cored off from and adjacent to the Phase 2 hole in order to sample the rocks lying close to the trace of the geological San Andreas Fault and across the SDZ and CDZ (Fig. 1c).

In Central California, the San Andreas Fault separates rocks located to the west belonging to the Salinian block from rocks located to the east referred to here as the Great Valley block, comprising units belonging to both the highly deformed, subduction-related Franciscan Complex and a Cretaceous forearc sedimentary sequence known as the Great Valley Group (Wakabayashi, 1999; Draper-Springer et al., 2009 and references therein). Close to the SAFZ at depth, the NE-dipping Phase 2 borehole cuts a thick sequence of arkosic sandstones and conglomerates inferred from detailed petrological, zircon fission track analyses and regional geological studies by Draper-Springer et al. (2009) to be of Paleocene-Eocene age. At 3157 m Md (as measured during Phase 2), an abrupt lithology change occurs as the borehole passes into a sequence of fine grained shales and siltstones (Bradbury et al., 2007), and at greater depths (below ca 3400 m Md) it passes into a siltstone-claystone sequence preserving Late Cretaceous fossils consistent with these being rocks belonging to the Great Valley Sequence (Draper-Springer et al., 2009). Most authors agree that the abrupt lithology change at 3157 m Md marks the location of the presently inactive (non-creeping) 'geological' San Andreas Fault that forms the eastern limit of the Salinian Block. However, the protolith affinities of the shale-rich rocks located between 3157 m and (at least) 3400 m Md are less certain. They coincide with an approximately 240 m wide region of low seismic velocities and resistivity interpreted to be the 'damage zone' of the SAFZ (Fig. 1d, left-hand image; Zoback et al., 2010; Jeppson et al., 2010). Three localised (metre-wide) zones located in the Phase 2 borehole at 3192 m (SDZ), 3302 m (CDZ) and 3413 m (NDZ = 'Northeast deformed zone') Md display even more markedly anomalous physical properties (Fig. 1d, right-hand image) and are thought to be active creeping and/or microseismically active faults.

3. The Phase 3 core

Approximately 40 m of 10 cm diameter rock core was recovered from ca 2.7 km vertical depth, sampling three key sections of the fault zone (Fig. 1c). The shallowest section of core comes from the Salinian Block (SB) wall rocks close to the trace of the geological San Andreas Fault (Hole E, core runs 1 and 2, with a length of ~11 m), whilst sections from the Great Valley Block (GVB) include the two actively creeping fault segments (Hole G, core runs 1–3, ~13 m long, including the SDZ; and Hole G, core runs 4–6, ~16 m long, including the CDZ) (SAFOD, 2010). The geological San Andreas Fault was not cored due to operational difficulties during drilling (Zoback pers. comm. 2007). Simplified summary logs of these three relatively continuous sections of core are presented in Fig. 1e–g. Note that as explained in the figure caption, the measured depths for each of the Phase 3 cores differ slightly from those recorded during Phase 2.

The lithological subdivision of the Phase 3 cores provides the geological and spatial context for the microstructural observations made from the 38 thin sections (for location see yellow dots in Fig. 1e–g) that form the main part of the paper. The cores can be most conveniently divided into three domain types:

1) Relatively undeformed *host rocks* (Fig. 2a–b; all of the core from Hole E [SB], most of the core from the deeper part of Hole G (part of core run 4, all of core runs 5–6 [GVB]);
2) Pervasively sheared regions of presently *'inactive' (not creeping) fault rocks* (Fig. 2c–e; parts of core run 2 and of all core runs 1 and 3, Hole G [GVB]);
3) Narrow, pervasively sheared regions of *actively creeping fault rocks*, the SDZ (lower part of core run 2, Hole G, Fig. 2f) and the CDZ (part of core run 4, Hole G).

The SDZ and CDZ in the core are both bounded by brittle faults. The other domain boundaries are not sampled by the existing core sections. Finally, it should be noted that the thin sections studied here were generally *not* oriented relative to the core, so it has not been possible to reconstruct either the directions of younging (e.g. Fig. 2b) or shear sense (e.g. Fig. 2c) observed in many samples.

3.1. Host rock domains: lithologies, mesostructure and microstructure

The Salinian block rocks sampled in core runs 1 and 2, Hole E, lie close to the projected trace of the geological San Andreas Fault at depth. The core materials comprise a sequence of green-grey, purple and red pebbly arkosic sandstones, together with a prominent, 1 m thick unit of dark grey siltstone-mudstone bounded at its base by a well defined fault (Fig. 1e). Bedding, defined by grainsize and compositional variations, iron oxide staining and by a crude alignment of pebble clasts, lies in a range of orientations relative to the axis of the core. Bedding laminations are offset by networks of minor faults arranged in a wide variety of orientations that carry dark red-brown, iron-stained zones of cataclasite up to 1 cm thick.

In thin section, the sandstones are predominantly (85–95%) composed of K-feldspar, plagioclase, and quartz, with subordinate grains of mica, ore, epidote and sphene, together with variable, but generally small (5–15%), amounts of illitic clay-rich matrix. The sandstone conglomerates are typically clast-supported, coarse to very coarse grained, with subrounded to subangular grain shapes and abundant pebble clasts (mainly feldspathic) locally up to 3 cm across (Fig. 2a). Individual sedimentary clasts are derived primarily from weakly deformed granitic protoliths as they preserve primary igneous textures and deformation features such as myrmekites and

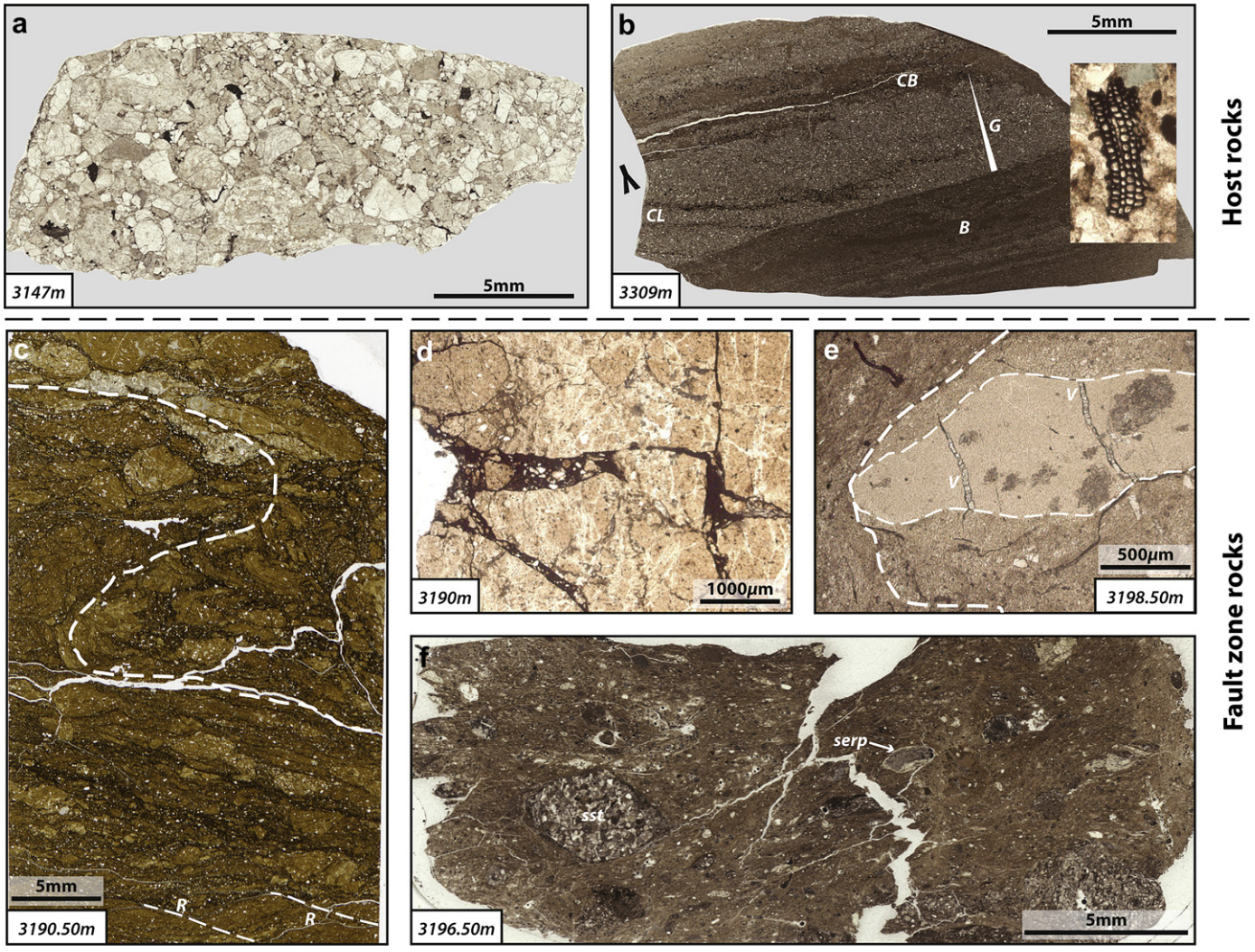

Fig. 2. Optical micrographs of typical host rock and fault zone rocks (with m Md given in metres) from the Phase 3 cores, all in plane polarised light. (a) Typical example of a coarse-grained arkosic sandstone that dominates the Salinian Block lithologies. Grain-scale microfracturing and minor faulting are widespread (e.g. Fig. 3a), but pervasive deformation is generally absent. (b) Laminated siltstone-mudstone host rock typical of the found in the Great Valley Block. Primary structures such as graded bedding (G), bioturbation (B), cross-lamination (CL) and convolute bedding (CB) give way up (see younging arrow). Microfossils (e.g. inset, with longest dimension of 200 μm) and carbonaceous materials are widespread. (c)–(e) Features of fault gouges in the inactive parts of the SAFZ from core runs 1–3, Hole G. (c) Mechanical shredding by folding and the development of Riedel-type shears deforming gouge materials derived from mudstones (brown) and subordinate sandstone lenses (pale). The mechanical comminution leads to the development of dark-brown-black gouge forming and interlinked network. Note that the sense of shear indicated by the Riedel shears and the folds are consistent throughout the thin section. (d) Black gouge similar to those seen in (c) hosted in fractures cutting a mudstone clast (?) – such features suggest that the gouges must have locally become fluidised and injected, presumably during periodic overpressuring events. (e) Clast of light brown mudstone enclosed within darker uniform gouge which is itself enclosed as a clast within a still darker foliated gouge. This sample comes from just outside the actively creeping region in core run 3, Hole G. Such features suggest multiple phases of shearing and gouge formation. The veins comprise intergrown fibrous calcite and anhydrite and are likely indicative of fluid-pressure-induced tensile fracturing events. They cut the two earlier gouges and are found as clasts in the youngest gouge. (f) Foliated gouge with clasts of sandstone (Sst) and serpentinite (Serp) from the active SDZ in core run 2, Hole G.

dynamic recrystallization of quartz. The siltstone–mudstone unit preserves fine-grained clay-rich matrix (95%) with isolated clasts of quartz, feldspar and chlorite (after biotite?).

Individual feldspar grains in sandstones are often weakly fractured, possibly due to the effects of tectonic compaction, but for the most part the sedimentary rocks lack pervasive deformation. In the sandstones, minor faults mostly display narrow (<mm-wide) zones of cataclasite, with local pressure solution seams (e.g. Fig. 3a). These give way in the lower part of the core from Hole E to broader (cm wide) diffuse zones of crushing, irregularly veined with calcite and ore; fibrous phyllosilicate (illite-smectite) also forms a minor, texturally early vein fill. Fluid-related alteration preferentially affects plagioclase grains which display highly sutured, curvilinear grain boundaries and internal alteration patches that host the growth of fine grained, irregular aggregates of phyllosilicate (illite-smectite). Aligned, fine- to ultrafine-grained aggregates (with individual grain basal lengths of mainly <1 μm) of smectitic phyllosilicate define the isolated solution seams preserved in fault-related sandstone-derived cataclasites and form much more extensive interconnected networks (up to 30 μm thick) in siltstone–mudstone host rocks (e.g. Fig. 4a). Here, BSE images (e.g. Fig. 4a inset) show that the strongly aligned smectitic phases (mainly illite-smectite based on EDX analyses, Fig. 5a) are preferentially developed along fracture surfaces, forming by the progressive replacement of existing matrix grains of phyllosilicate, as well as forming new fibrous overgrowths around host rock clasts. Host rock clasts of quartz and feldspar are noticeably rare in these aligned networks of phyllosilicate and are often sharply

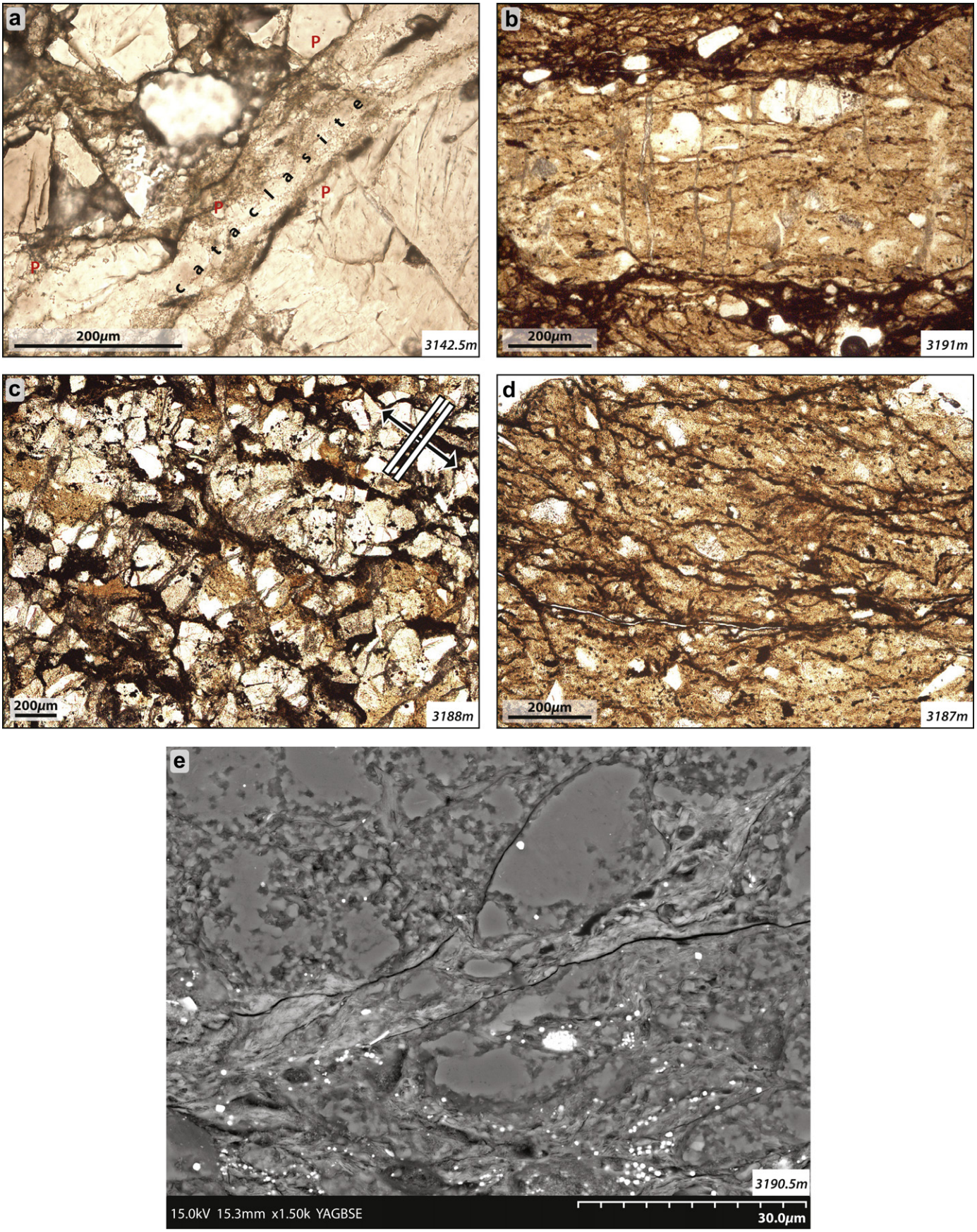

Fig. 3. Illustrative examples of textures consistent with the operation of stress-induced solution-precipitation and diffusive mass transfer processes in the SAFOD fault rocks (with Md given in metres). (a)–(d) are optical images in polarised light. (e) is a BSE image from the SEM. (a) Discontinuous, dark pressure solution seams (labelled 'P') associated with

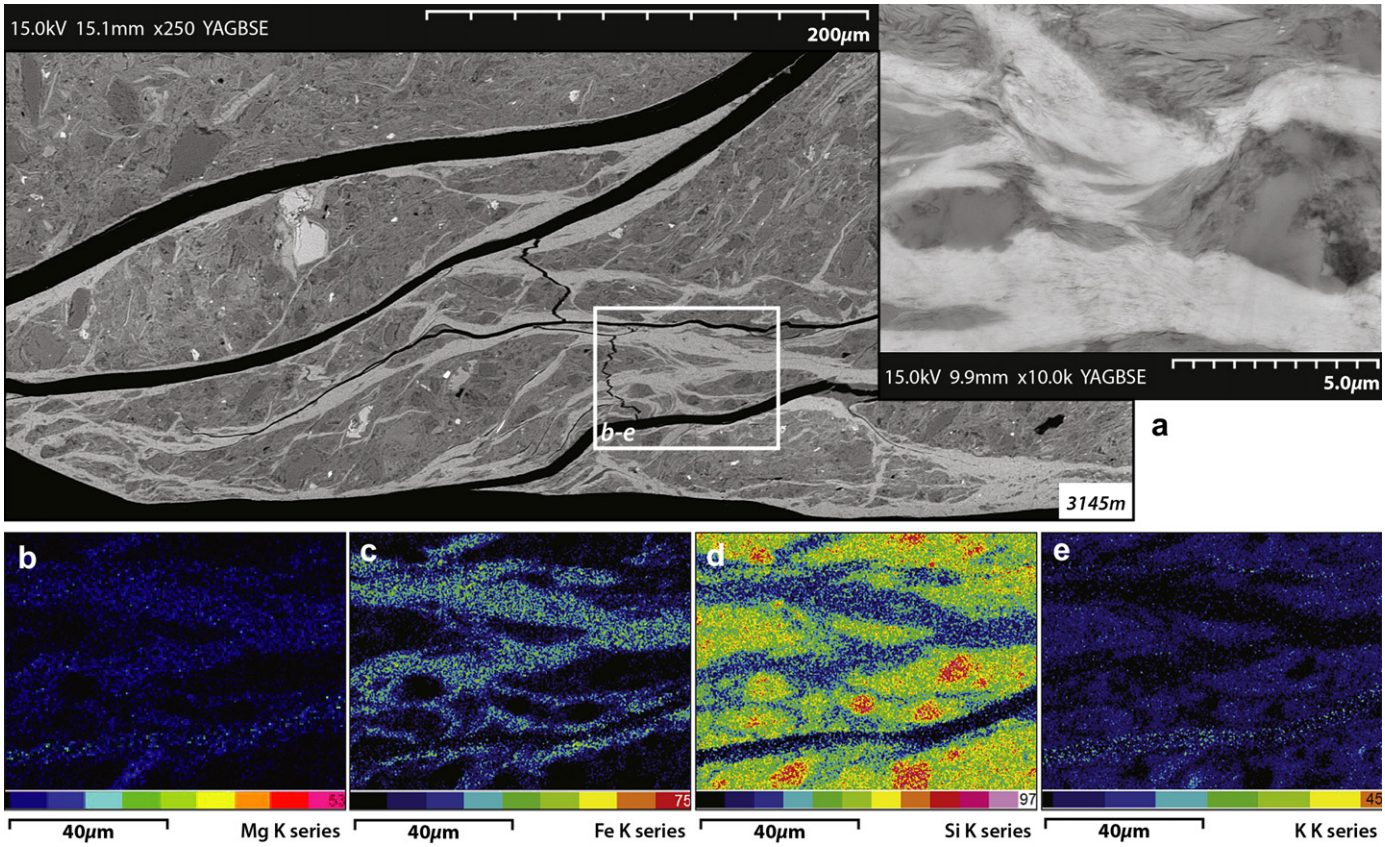

Fig. 4. Textural and compositional changes associated with smectitic phyllosilicate growth along brittle fractures in a mudstone from the Salinian Block (core run 1, Hole E). (a) BSE image showing the interconnected network of pale smectitic phyllosilicate (illite-Smectite – see Fig. 5a) cutting otherwise little deformed Salinian mudstone unit. White box indicates location of EDX compositional maps in (b)–(e). Inset shows typical phyllosilicate texture at higher magnification, with highly partitioned distribution of dark detrital illitic phyllosilicates and pale authigenic smectitic phyllosilicates. Note general absence of pale smectitic phases in host material, truncation of quartz grains (e.g. bottom left) and partial replacement of darker, more illite-rich detrital grains (e.g. centre of image). (b)–(e) EDX compositional maps (normalised weight percentages) showing that the development of the pale smectitic phyllosilicate layers is associated with relative enrichment in iron and magnesium and relative depletion in silicon and potassium.

terminated at their margins (see Fig. 4a inset). Such textures strongly suggest that a significant amount of the smectitic phyllosilicate is authigenic and syn-tectonic, with fluid assisted, stress-induced solution-precipitation processes taking place. EDX compositional maps suggest significant enrichments in Mg and Fe and depletion in Si and K relative to the host rocks during smectitic phyllosilicate development (Fig. 4b–e).

The rocks sampled from the Salinian block in the core runs from Hole E are lithologically similar to the Paleocene-Eocene sequence described from the Phase 2 borehole by Draper-Springer et al. (2009). As noted by these authors from Phase 2 materials, the composition and relict igneous and crystal plastic deformation textures preserved widely in the sandstone detrital clasts suggest that the sedimentary rocks were primarily derived from a Salinian granitoid basement source.

The Great Valley block rocks sampled in core runs 4–6 from the lower part of Hole G include the fault-bounded active CDZ, but otherwise preserve a sequence of interbedded fine grained grey sandstones, siltstones and mudstones, with the latter forming over 50% of the sampled core material (Fig. 1g). Centimetre– to metre-scale compositional layering and finer bedding laminations are defined by grainsize and compositional variations and are generally oriented at high angles to the axis of the core. Many primary sedimentary features indicative of way up are preserved, together with microfossils (e.g. Fig. 2b). Complex arrays of minor faults occur in a variety of orientations throughout the core, but a majority of the larger faults lie at low angles to bedding and high angles to the axis of the core (Fig. 1g). Mostly mm-thick calcite and (less commonly) anhydrite or smectitic phyllosilicate veins occur as infillings in boudinaged sandstone units and in dilatational pull-apart features developed along minor faults. A more extensive network of generally bedding-parallel calcite and anhydrite veins occurs in the dark siltstone-mudstone unit that immediately underlies the active CDZ (Fig. 1g). Cm– to m-scale asymmetric folds are developed in the lowermost part of the core sampled from Hole G (Fig. 1g; core run 6).

a narrow zone of quartzofeldspathic cataclasite along a minor fault cutting sandstones from the Salinian Block, core run 1, Hole E. (b) Veins of calcite cutting brown shale-derived gouge cross-cut by later dark-brown – black gouge, core run 2, Hole G. Note isolated dark pressure solution seams and tabular shapes of white quartz grains due to the effects of dissolution. (c) Impure sandstone unit cut by dark pressure solution seams and orthogonal calcite and smectitic phyllosilicate veins, core run 1, Hole G. The general orientation of the veins (white bars), pressure solution seams (black line) and vein opening directions inferred from mineral fibre directions in veins (arrow heads) are shown top right of the image. (d) Shale-derived gouge with interconnected dark pressure solution seams, core run 1, Hole G. (e) BSE image of typical pressure solution seam with aligned aggregates of pale smectitic phyllosilicate wrapping clasts in cataclastic gouge unit, core run 2, Hole G. Note the pair of sub-parallel cracks bounding the solution seam and interpreted to be the result of water loss during coring or thin section preparation. (For interpretation of the references to colour in this figure legend, the reader is referred to the web version of this article)

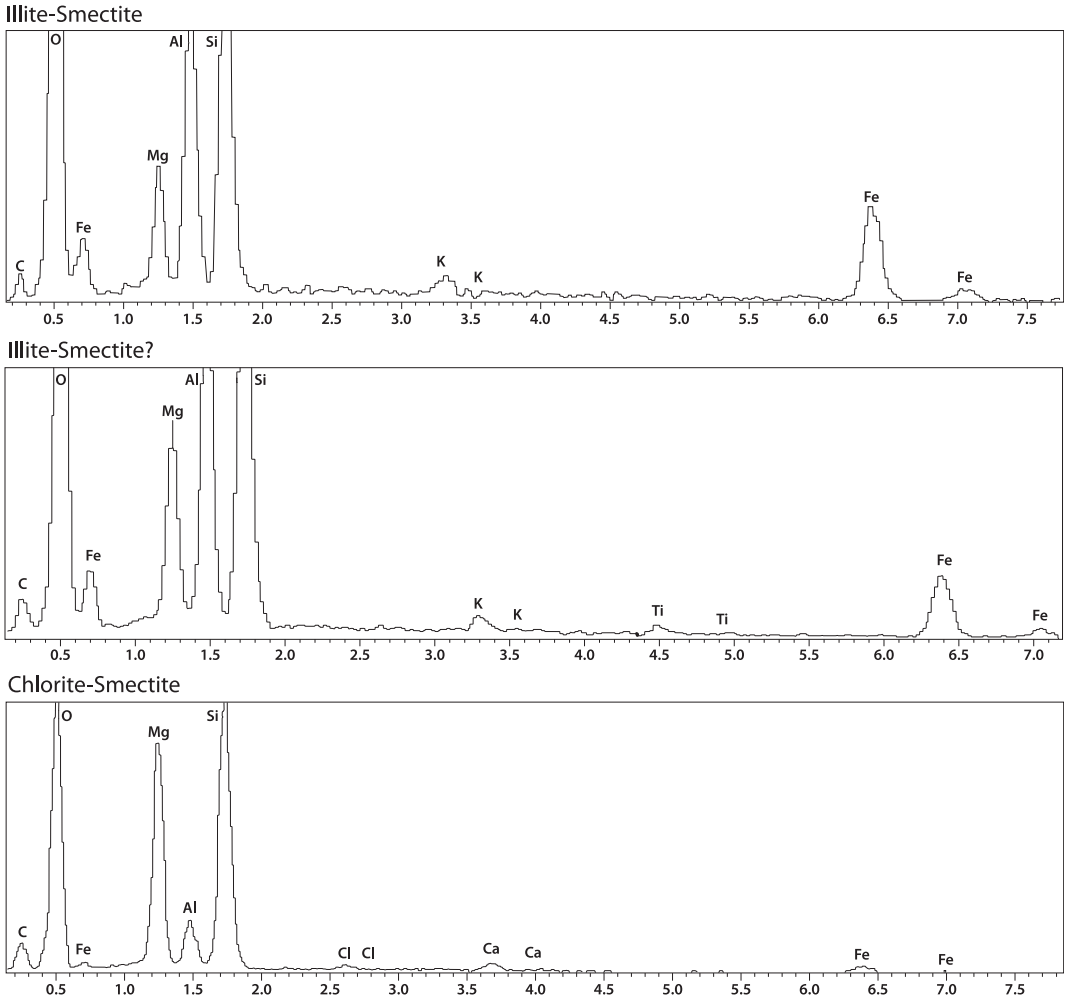

Fig. 5. Representative EDX traces derived from smectitic phyllosilicate grains in: a) core run 1, Hole E (Fig. 4b) core run 1, Hole G (Fig. 2c andFig. 6a,b and c) core run 4, Hole G (Fig. 6e and f).

In thin section, the shales are generally reddish-brown, comprising a fine clay matrix with isolated clasts of quartz, feldspar, mica and flakes of organic, carbonaceous material. Possibly authigenic grains and aggregates of fine grained pyrite are locally common. The phyllosilicate grains are generally aligned into a weak foliation and XRD analyses suggest that these include chlorite, illite and mixed layer phases (illite-smectite, chlorite-smectite) (Schleicher et al., 2009a,b, 2010; SAFOD, 2010). Siltstones and sandstones are predominantly matrix-supported, containing up to 50% clasts (mostly quartz and feldspar), with the local development of calcite and smectitic phyllosilicate mineral cements in patches. The sedimentary rocks are uniformly low grade, with the mineral assemblages described above being wholly consistent with the low temperatures recorded in the deeper parts of the Phase 2 borehole (100–120 °C; Mittempergher et al., 2009).

Minor faults typically are associated with sub-mm wide zones of weakly foliated cataclasite, with, sub-micron-scale flakes of authigenic smectitic phyllosilicate overgrowing clasts. Larger faults display millimetre– to centimetre-thick foliated gouges rich in smectitic phyllosilicate, with chaotic millimetre to micron-scale folds and brittle slip surfaces suggesting later shear localisation events. Carbonate veins are common in small (<1 mm-thick) dilatational pull-aparts along faults and are commonly locally internally deformed by cataclasis, presumably during later slip events along pre-existing slip surfaces.

3.2. Fault rock domains: lithologies, mesostructure and microstructure

The 'inactive', non-creeping fault rocks from the westernmost part of the GVB are sampled in core runs 1–3, from the upper part of Hole G which also is cut by the fault-bounded active SDZ (Fig. 1f). The rocks are predominantly foliated cataclasites and gouges derived mainly from an argillaceous host rock of a mineralogically similar composition to the GVB host rocks preserved in core runs 4–6 lower down in Hole G. Boundinaged layers of laminated sandstone up to 10 cm thick, with mm-to cm-thick calcite and (less commonly) anhydrite mineral vein infills are preserved in the least deformed upper and lower parts of core runs 1 and 3, respectively, in Hole G (e.g. top of Fig. 2c; see also Mittempergher et al., 2009). The remaining rocks are dark grey foliated gouges which become increasingly dark in colour and highly indurated in the region immediately above the active SDZ (Fig. 1f). The foliation throughout is relatively constant in orientation and lies at moderate to high angles to the axis of the core.

In thin section, a significant variety of gouges is observed. Less deformed types display clear relicts of bedding and compositional layering (e.g. lenses of sandstone set in mudstones) affected by asymmetric minor folds and Riedel-type shears (e.g. Fig. 2c). Associated grain-scale disaggregation and abrasion help to progressively dismember and mechanically intermix host rock units and lead to the development of interconnected networks of

dark-brown black gouge (e.g. Fig. 2c). Compositionally similar units of black gouge are seen to locally infill irregular fracture networks cutting more intact regions of shale (e.g. Fig. 2d) and appear to have been injected, presumably under enhanced fluid pressures. Sub-mm to cm-scale networks of mainly calcite and subordinate anhydrite veins are preserved that formed prior to, during and after local gouge forming events (e.g. Fig. 3b). More evolved gouges can appear rather more texturally homogeneous on first inspection, but the localised preservation of clasts within clasts (e.g. Fig. 2e) points to a protracted history of multiple brecciation and re-brecciation.

There is widespread textural evidence for the operation of grain-scale fluid-assisted diffusive mass transfer processes. Dark pressure solution seams are preserved in both sandstones and shales (Fig. 3c and d, respectively), and in the former lithology, are associated with calcite veins filling intergranular fractures oriented orthogonally to the pressure-solution seams (Fig. 3c). The solution seams are defined by the growth of aligned, fibrous aggregates of ultrafine-grained smectitic phyllosilicates that wrap around pre-existing clasts (Fig. 3e). The development of the brown-black gouges by cataclasis is also intimately associated with a volumetrically more pervasive growth of fine- to ultrafine-grained interconnected networks of smectitic phyllosilicate (Fig. 6a and b; mainly Fe–Mg illite-smectite, Fig. 5b). These observations demonstrate that during gouge development, stress-induced solution-precipitation creep processes are closely associated with cataclasis and grain-scale fluid pressure-induced fracturing, as speculated by Schleicher et al. (2009b, 2010). Many of the inactive, non-creeping fault gouges – and especially the blackest types – are additionally characterised by the widespread growth of fine disseminated grains of relatively late-stage authigenic pyrite (e.g. Figs 3e,6a–c).

The active creeping fault rocks sampled in core runs 2 and 4, Hole G, are 1–2 m wide, fault-bounded units that are quite distinct from the other fault rocks on both lithological and textural grounds. The rocks are dark grey-green foliated gouges with a highly distinctive scaly fabric with numerous polished and striated foliation surfaces (e.g. SAFOD, 2010). They contain a wide variety of rounded clasts, some up to several tens of cm across, most particularly of green serpentinite cut by numerous calcite veins, a clast type not found out with of the active shear zones (Figs. 1f and g, 2f). Other clast types include sandstones, siltstones and mudstones similar to the adjacent GVB lithologies, crystalline carbonate and some possible granitic units. In sharp contrast to the inactive gouges, where mineral veins are intergranular and continuous, in active gouges mineral veins only occur as individual clasts or inside clasts of other lithologies, including serpentinite. Sills et al. (2009) have used X-ray Computed Tomography imaging to investigate the mesoscale structure of the active gouge core samples. They have shown that the clasts in the gouge have a strong shape preferred orientation, with long axes oriented sub-parallel to the SAFZ and that the observed uniformity in porphyroclast shapes and sizes is consistent with distributed deformation during aseismic creep.

In optically imaged thin sections and under the SEM, samples of these foliated gouge units are particularly distinct due to the widespread development of foliation-parallel, curviplanar interlinked networks of micron-scale cracks (e.g. the black features seen in the SEM images shown in Fig. 6d and e), features likely formed following coring and possibly during thin section preparation (see below). The foliation is typically phacoidal, with asymmetric textures (shear bands, sigma-porphyroclasts) and often disharmonic folds on centimetre to micron-scales (e.g. Fig. 6e and f). The gouge matrix is completely dominated by the development of fine– to ultrafine-grained aligned aggregates of Mg-rich smectitic phyllosilicate (chlorite-smectites, possibly corrensite and/or saponite, Fig. 5c; see also SAFOD, 2010) which now forms over 50% of the total rock volume. Locally, the development of multiple generations of smectitic phyllosilicate is evident from the brecciation of earlier grains and their overgrowth by new fibrous grains suggesting cyclic alternations in solution-precipitation creep processes and cataclasis.

Given the widespread presence of smectitic phases in the active gouges, it is suggested that the curviplanar crack networks likely reflect dewatering and volume loss in the clays during core sampling and thin section preparation. The rocks tend to break along these surfaces which display the characteristic polished and striated appearance. Contrary to the views expressed by some authors (e.g. Schleicher et al., 2010), there is nothing particularly unusual about the presence of such features in rocks of this composition. Analogous features are seen, for example, along shear fractures developed in smectite-rich clay soils formed due to seasonally controlled swelling and shrinking behaviour (Van Breemen and Buurman, 2002). Similar, but less intensely developed cracks are also associated with smectitic phyllosilicate-rich rocks in both the inactive gouges and along some minor faults cutting host rock units (e.g. see Figs. 3e and 4a, respectively).

The textural and mineralogical differences between the inactive and active gouge domains are strikingly emphasised by the results of EDX compositional mapping (Fig. 7). The active gouges are markedly enriched in Mg and depleted in Si compared to the immediately adjacent unit of inactive gouge that is located less than half a metre away. Relative enrichments in iron and depletion in potassium (as seen in smectite-rich gouges in the inactive segments, e.g. Fig. 4c and e) are not observed in the actively creeping gouges. Further detailed X-ray diffraction analyses, TEM and microprobe analyses are clearly required in order to properly characterise the mineralogy and compositional distribution of the smectitic phyllosilicate phases present within both inactive and active fault gouges from the Phase 3 SAFOD core.

4. Discussion

In the absence of a comprehensive microstructural, microanalytical and geochronological study of all of the Phase 3 SAFOD core materials, it is important to recognise that at present, only deformation features seen in the actively creeping shear zones can be attributed to SAFZ movements with reasonable certainty. The results of 40Ar/39Ar dating of illites in SAFOD samples carried out by Schleicher et al. (2010) have yielded Miocene (8 ± 1.3 Ma) to Pliocene (4 ± 4.9) ages consistent with earlier phases of fault movement. Nevertheless, it is still conceivable that some of the deformation features seen in the host rocks and inactive, non-creeping gouges may entirely pre-date the development of the SAFZ, particularly if deformed rocks derived from the subduction-related melanges of the Franciscan Formation are entrained within the fault zone (e.g. Evans et al., 2009; Bradbury and Evans, 2009). In our opinion, the observed textural and mineralogical continuity of the GVB host rocks and gouges argues against such a possibility, as does the absence of relict high pressure metamorphic minerals such as jadeite, pumpellyite or glaucophane which typify rocks of the Franciscan Formation (e.g. Bailey et al., 1964; Ernst, 1973). In the following discussion, we will therefore assume that all the deformational and mineralogical processes observed in all the fault rocks are related to fault movements during the history of the SAFZ.

Previous studies carried out during Phases 1 and 2 of the SAFOD drilling have shown that high pore fluid pressures are not currently developed in the fault zone (e.g. Zoback et al., 2010), whilst Helium gas isotopic analyses from within the borehole reveal significant differences in the 3He/4He ratios either side of the fault core suggesting that it acts as a regional fluid seal (Wiersberg and Erzinger, 2008). This seems consistent with the observed clay-rich nature of

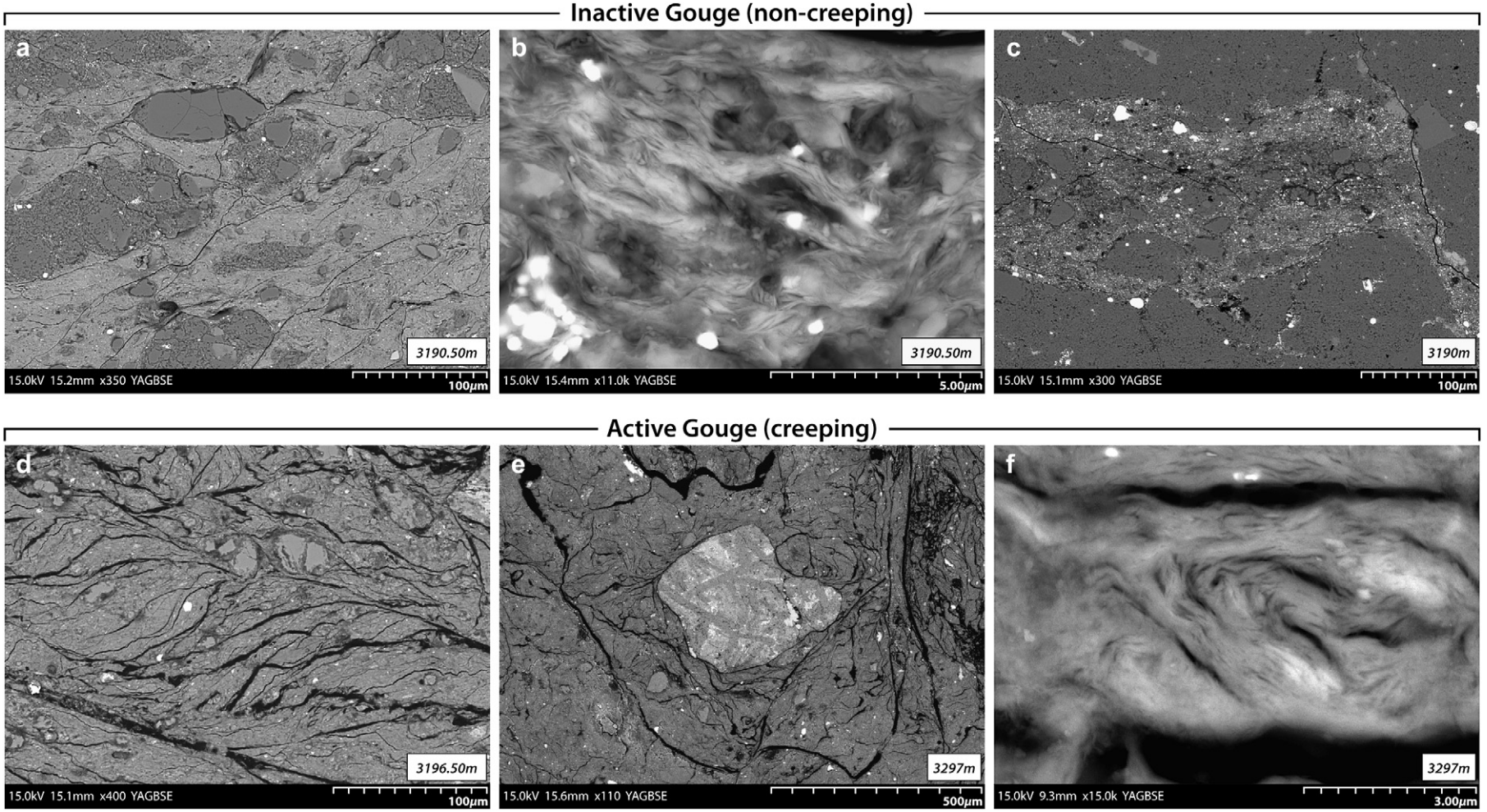

Fig. 6. BSE images of typical textures associated with smectitic phyllosilicate growth in inactive, non-creeping (a–c) and active creeping shear zones (d–f) of the SAFZ. (a–b) Sub-millimetre- to nanometre-scale development of pale smectitic phyllosilicate networks (illite-smectite – see Fig. 5b) wrapping and overgrowing brittle gouge/cataclasite and mineral clasts. These materials form the dark-brown-black gouges shown in Fig. 2c. Note the widespread growth of late stage, micron-scale grains of bright pyrite. (c) BSE image of injected black gouge shown in Fig. 2d. Note the bright disseminated pyrite grains which are largely restricted to the injected gouge (cf. a and b above). (d) Lower power view of typical asymmetric fabrics (shear bands, sigma clasts) in active SDZ gouges. Note again the foliation-parallel, curviplanar networks of cracks consistent with dewatering of the smectite-rich matrix during section preparation and the apparent brecciation of gouge along some of the shear band surfaces (e.g. bottom right). (e) Lower power view of smectitic phyllosilicate-rich, chaotically foliated gouge (again with dewatering cracks) surrounding a serpentinite clast from the active CDZ. Note the local brecciation of the gouge along some slip surfaces (e.g. right-hand side). (f) High power image of micron-scale folds in smectitic phyllosilicate aggregates (chlorite-smectite – see Fig. 5c).

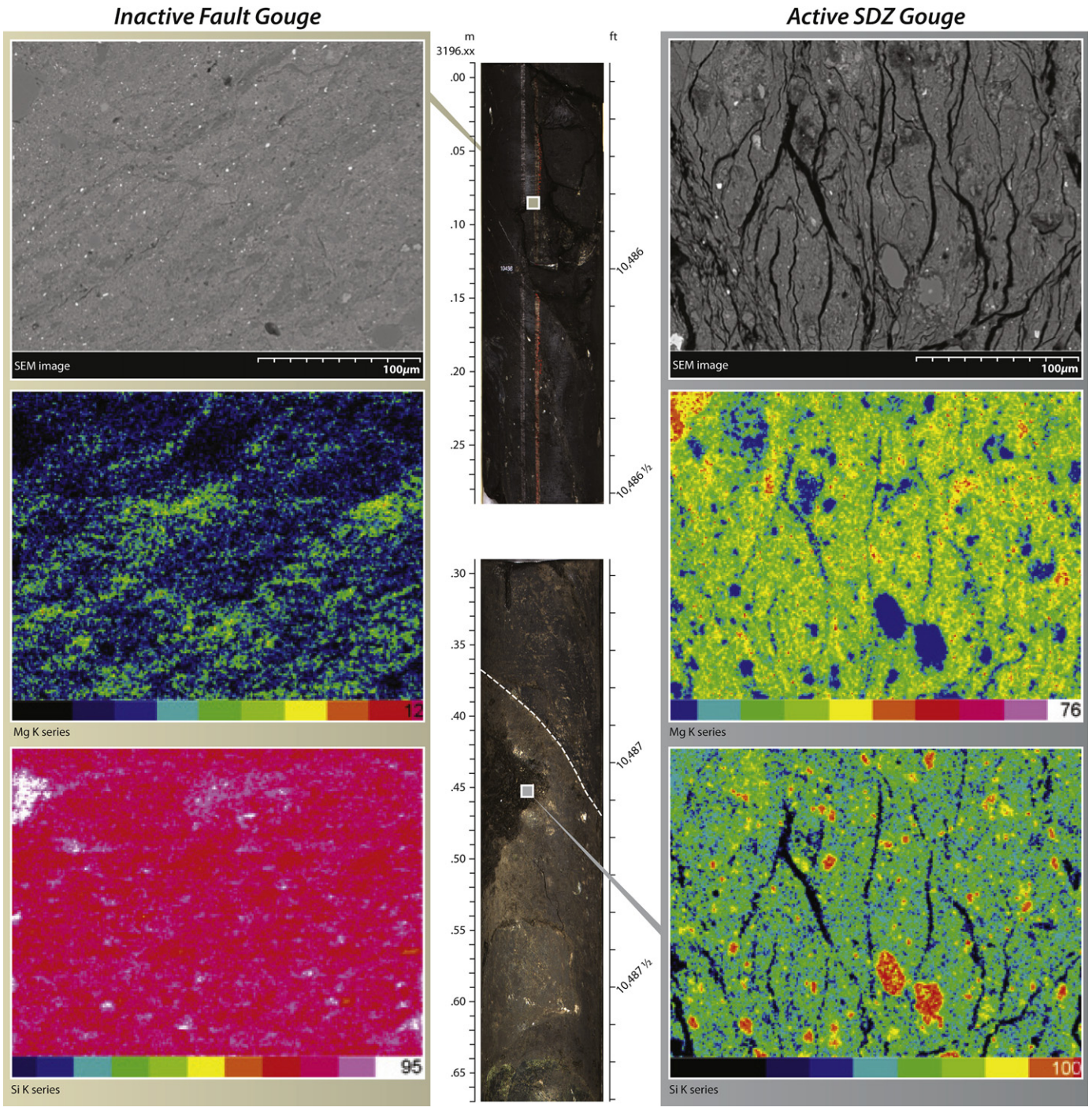

Fig. 7. Major textural and compositional changes across the upper contact of the active SDZ (Hole G, core run 2). The central part of the image shows photographs of the relevant sections of core (which are continuous with one another). Either side are SEM images (top left and right) and EDX compositional maps (normalised weight percentages) for magnesium and silicon for inactive gouge (to the left) and active SDZ gouge (to the right). Note: i) the curviplanar networks of foliation-parallel cracks consistent with dewatering of the smectite-rich matrix of the active SDZ gouge during section preparation (see also Fig. 6d and e); and ii) that the active gouge shows very significant enrichment in magnesium and depletion in silicon relative to the inactive gouge.

the gouges and with the lack of mineral veins in the currently creeping, active shear zone gouges (SDZ, CDZ). Conversely, the widespread preservation of veins both in the host rocks and inactive fault gouges of the GVB suggest that elevated fluid pressures may have existed on many occasions in the geological past if we assume that all the textures in the latter rocks are related to deformation along the SAFZ.

During Phase 2 drilling, the occurrence of talc fragments, associated with serpentinite was recorded in isolated rock chip samples by Moore and Rymer (2007). Talc is stable over a wide range of pressure and temperature conditions, has a very low friction coefficient (ca 0.2) and displays velocity strengthening behaviour. It has therefore been suggested that the development of this mineral phase could account for the low mechanical strength of at least the Parkfield creeping segment of the San Andreas Fault. During the present study of all 38 thin sections from SAFOD, few grains of talc were identified in any of the Phase 3 core samples and so this hypothesis remains unproven.

A range of other, potentially weak minerals were identified in rock chippings recovered during the Phase 2 drilling, including illite and chlorite, together with illite-smectite and chlorite-smectite mixed layer clays, including possibly both corrensite and saponite (e.g. Solum et al., 2006; Schleicher et al., 2009a,b 2010; SAFOD, 2010). The mixed layer smectitic phases are particularly significant as numerous experimental studies have shown that the presence of such hydrous mineral phases can substantially reduce the shear strength of rocks (e.g. Wang, 1984; Saffer et al., 2001; Saffer and Marone, 2003; Morrow et al., 2007).

Based on analyses of fault rock chips recovered during drilling and coring, Schleicher et al. (2006, 2010) refer to the presence and development of thin so-called 'nanocoatings' of smectite along slip surfaces. Our analysis of the thin sections taken from the intact core (e.g. Fig. 5a–f) demonstrates that the development of smectitic phyllosilicates is far more widespread than is implied by these authors and that in the actively creeping gouges, they form the *dominant* matrix minerals. Deformation experiments carried out on powdered samples rich in these minerals consistently show reduced friction coefficients, in some cases as low as 0.3 (Tembe et al., 2006; Morrow et al., 2007; Carpenter et al., 2009). The observed pervasive development of interconnected networks of strongly aligned phyllosilicate phases is particularly important as this can significantly enhance the upscale transfer of grain-scale weakening effects (Wintsch et al., 1995; Holdsworth, 2004). In laboratory-based deformation studies carried out in talc-rich fault rocks, Collettini et al. (2010) have shown that experiments carried out on intact fault rock wafers, where the interconnected network of weak phyllosilicates is preserved, yield significantly lower friction coefficients compared to powdered samples of the same fault rocks. On this basis, it is reasonable to propose that future measurements of friction carried out on intact rock wafers of the smectite-rich SAFZ fault gouges will probably yield friction coefficients lower than 0.2, the value predicted by existing stress and heat flow data (e.g. Moore and Rymer, 2007). The apparent weakness of the SAFZ gouges is more generally attested to by the observation that deformation – including the current creep displacements – has clearly localised into the relatively narrow regions of gouge that contain the highest proportions of smectitic phyllosilicates, especially Mg-rich varieties.

The observed textural relationships and compositional maps (e.g. Figs. 3–7), together with the geochemical studies of Schleicher et al. (2009a,b) suggest that the development of the phyllosilicate-rich fault rocks is associated with the widespread operation of stress-induced solution-precipitation and mass transfer processes. This makes it possible that processes other than frictional sliding (*sensu stricto*) have contributed to fault weakening and creep along the SAFZ. There is abundant evidence from theoretical and experimental studies (e.g. Mares and Kronenberg, 1993; Bos and Spiers, 2000, 2002; Bos et al., 2000a,b; Niemeijer and Spiers, 2005; Jefferies et al., 2006b) that the onset of diffusive mass transfer mechanisms in phyllosilicate-rich fault rocks can lead to profound weakening in fault zones. The closely associated processes of cataclasis and the growth of fine– to ultrafine-grained aggregates of authigenic phyllosilicates in the gouges will help to facilitate the operation of grainsize-sensitive diffusive mass transfer mechanisms at strain rates that will make a significant contribution to the active creep of 2.5 cm/year observed along the Parkfield segment of the SAFZ.

Recent geological studies of the exhumed deeper parts of old crustal-scale structures elsewhere in the world, such as repeatedly reactivated faults and low angle normal faults, suggest that weakening in narrow fault cores is also related to the development of foliated, phyllosilicate-rich fault rocks following cataclasis (e.g. Wintsch et al., 1995; Imber et al., 1997; Gueydan et al., 2003; Collettini and Holdsworth, 2004; Jefferies et al., 2006a,b). In several examples, the growth of Mg-rich phyllosilicates can be directly related to weakening (e.g. Mg-chlorite in the MTL, Japan, Jefferies et al., 2006a; talc in the Zuccale Fault, Italy, Collettini et al., 2009, 2010). This suggests that the processes recognised along the SAFZ in the SAFOD borehole are of direct relevance to a more general understanding of weakening in all crustal-scale fault zones.

5. Conclusions

Based on our microstructural study of 38 thin sections from the Phase 3 SAFOD core, we conclude that the SAFZ preserves a suite of fault rocks showing evidence for the operation of upper crustal fluid-related fault weakening and chemical alteration processes. Minor faults cutting the host rocks display classical brittle deformation processes involving repeated cycles of cataclasis, pressure solution and fluid pressure-induced fracturing. The resulting mineral veins (calcite, anhydrite) formed prior to, during and after local fault rock-forming deformation episodes.

The 'signature' fault zone process in the larger displacement faults associated with the SAFZ is the development of foliated cataclasites and gouges comprising interconnected networks of low friction smectitic phyllosilicates (μ likely <0.3). Talc is largely absent in the thin sections examined during the present study. Outwith of the actively creeping shear zones, the smectite-enrichment is most likely related to fluid–rock interactions, with marked enrichments in Mg, Fe and depletions in Si and K observed. Along more minor faults in host rocks, there is a strong compositional control on the intensity of smectitic phyllosilicate development, but alteration becomes more widespread in larger displacement fault gouges. The development of smectitic phyllosilicate becomes ubiquitous in the actively deforming serpentinite clast-bearing gouges. Here the chemical alteration associated with smectite growth is significantly different, displaying a more marked enrichment in Mg and depletion in Si compared to the adjacent inactive gouges. The enrichment in disseminated pyrite observed in the wall rocks immediately above the SDZ in core run 2, Hole G (Fig. 1f) may also indicate some loss in Fe from the actively creeping shear zones. The close spatial association between the presence of serpentinite clasts and the ubiquitous growth of markedly Mg-rich smectites may indicate a genetic link between these two features. Speculatively, the weakening required in order to develop the actively creeping shear zones may have been triggered by a relatively recent influx of Mg-rich fluids that have interacted with the serpentinite bodies entrained within the SAFZ (cf. Moore and Rymer, 2007). The lack of mineral veins in the gouge matrix of the shear zones implies that any such influx was localised, gradual and was not obviously facilitated by the widespread development of fluid-induced fracture systems.

It is important to end with a note of caution: the development of smectitic phyllosilicate-rich fault rocks on its own does not provide an explanation for the overall weakness of crustal-scale faults such as the SAFZ which extend down to depths of 15 km or more. It is generally agreed that smectitic low friction clays such as saponite will break down at temperatures not much greater than those encountered close to the bottom of the SAFOD borehole (ca. 100–120 °C) where they are likely to be replaced by minerals with higher friction coefficients, e.g. Mg-chlorite (Frey and Robinson, 1999). Thus the development of such clays only represents a plausible weakening mechanism for faults in the uppermost part of the crust (0–5 km depth). At greater depths and higher temperatures, other processes, such as stress-induced solution-precipitation creep may become more important leading to so-called 'frictional-viscous flow' (e.g. Bos and Spiers, 2000,2002; Jefferies et al., 2006a,b). More generally, geological studies of crustal-scale weak faults have shown that the growth of

interconnected networks of weak phyllosilicates reflects a complex and protracted interaction between fluid-assisted deformation processes such as hydrofracture, cataclasis, stress-induced solution-precipitation and frictional sliding. Each may lead to weakening effects operating on different timescales, but it is their combination that ultimately leads to the development of faults that are weak in an absolute sense.

Acknowledgements

The authors would particularly like to thank the following for their help and discussions during the preparation of this paper: Jim Evans, Kelly Bradbury, Anja Schleicher, Steve Smith, André Niemeijer, Silvia Mittempergher, Mark Zoback, and Chris Marone. Steve Hickman is due special thanks for numerous discussions and help that go well beyond what might reasonably be expected. We are also grateful for the constructive and informative reviews provided by Diane Moore and an anonymous reviewer, together with the editorial guidance of Cees Passchier. The views expressed here are, however, entirely the responsibility of the authors. REH gratefully acknowledges the receipt of a Leverhulme Research Fellowship during the preparation of this paper.

References

Allen, C.R., 1981. The modern San Andreas fault. A Symposium in Honour of, In: Rubey, W.W., Ernst, W.G. (Eds.), The Geotectonic Development of California. Prentice Hall, Englewood Cliffs, New Jersey, pp. 511–534.

Bailey, E.H., Irwin, W.P., Jones, D.L., 1964. Franciscan and related rocks, and their significance in the geology of western California. California Division of Mines Geological Bulletin 183, 171.

Boness, N.L., Zoback, M.D., 2006. A multi-scale study of the mechanisms controlling shear velocity anisotropy in the San Andreas Fault Observatory at depth. Geophysics 7 (5), F131–F146.

Bos, B., Peach, C.J., Spiers, C.J., 2000a. Frictional-viscous flow of simulated fault gouge caused by the combined effects of phyllosilicates and pressure solution. Tectonophysics 327, 173–194.

Bos, B., Peach, C.J., Spiers, C.J., 2000b. Slip behaviour of simulated gouge-bearing faults under conditions favoring pressure solution. Journal of Geophysical Research 105, 16699–16717.

Bos, B., Spiers, C.J., 2000. Effect of phyllosilicates on fluid-assisted healing of gouge-bearing faults. Earth and Planetary Science Letters 184, 199–210.

Bos, B., Spiers, C.J., 2002. Frictional-viscous flow of phyllosilicate-bearing fault rock: microphysical model and implications for crustal strength profiles. Journal of Geophysical Research 107, 2028. doi:10.1029/2001JB000301.

Bradbury, K.K., Barton, D.C., Solum, J.G., Draper, S.D., Evans, J.P., 2007. Mineralogic and textural analyses of drill cuttings from the San Andreas Fault Observatory at Depth (SAFOD) boreholes: initial interpretations of fault zone composition and constraints on geologic models. Geosphere 3 (5), 299–318. doi:10.1130/GES00076.1.

Bradbury, K.K., Evans, J.P., 2009. Franciscan formation within the SAFOD borehole, near Parkfield, CA. In: Geological Society of America, Abstracts and Programs, vol. 41, p. 404.

Brune, J.N., Henyey, T.L., Roy, R.F., 1969. Heat flow, stress, and rate of slip along the San Andreas fault, California. Journal of Geophysical Research 74, 3821–3827.

Carpenter, B.M., Marone, C., Saffer, D.M., 2009. Frictional behavior of materials in the 3D SAFOD volume. Geophysical Research Letters 36. doi:10.1029/2008GL036660.

Collettini, C., Holdsworth, R.E., 2004. Fault zone weakening and character of slip along low-angle normal faults: insights from the Zuccale fault, Isle of Elba, Italy. Journal of the Geological Society of London 161, 1039–1051.

Collettini, C., Niemeijer, A.R., Viti, C., Marone, C., 2009. Fault zone fabric and fault weakness. Nature 462, 907–910.

Collettini, C., Niemeijer, A.R., Viti, C., Marone, C., 2010. Mechanical behaviour of phyllosilicate-rich faults. Geophysical Research Abstracts 12 (EGU 2010–10139).

Draper-Springer, S., Evans, J.P., Garver, J.I., Kirschner, D., Janecke, S.U., 2009. Arkosic rocks from the San Andreas fault Observatory at depth (SAFOD) borehole, central California; implications for the structure and tectonics of the San Andreas fault zone. Lithosphere 1, 206–226.

Ernst, W.G., 1973. Blueschist metamorphism and PT regimes in active subduction zones. Tectonophysics 17, 255–272.

Evans, J.P., Jeppson, T.N., Bradbury, K.K., Lowry, A.R., 2009. Evaluation of fault zone structure and properties at depth, with insights into deformation and alteration of the San Andreas Fault at SAFOD. Eos Transactions of the American Geophysical Union 90 (52) Fall Meeting Supplement, Abstract T14B-03.

Frey, M., Robinson, D., 1999. Low-grade Metamorphism. Blackwell Science, Cambridge, p. 313.

Gueydan, F., Leroy, Y.M., Jolivet, L., Agard, P., 2003. Analysis of continental mid-crustal strain localization induced by microfracturing and reaction-softening. Journal of Geophysical Research 108. doi:10.1029/2001JB000611.

Hickman, S., Zoback, M.D., 2004. Stress orientations and magnitudes in the SAFOD pilot hole. Geophysical Research Letters 31 (L15S12). doi:10.1029/2004GL020043.

Holdsworth, R.E., 2004. Weak faults – rotten cores. Science 303, 181–182.

Imber, J., Holdsworth, R.E., Butler, C.A., Lloyd, G.E., 1997. Fault-zone weakening processes along the reactivated outer hebrides fault zone, Scotland. Journal of the Geological Society of London 154, 105–109.

Jefferies, S.P., Holdsworth, R.E., Shimamoto, T., Takagi, H., Lloyd, G.E., Spiers, C.J., 2006a. Origin and mechanical significance of foliated cataclastic rocks in the cores of crustal-scale faults: examples from the Median Tectonic Line, Japan. Journal of Geophysical Research 111. doi:10.1029/2005JB004205.

Jefferies, S.P., Holdsworth, R.E., Wibberley, C.A.J., Shimamoto, T., Spiers, C.J., Niemeijer, A.R., Lloyd, G.E., 2006b. The nature and importance of phyllonite development in crustal-scale fault cores: an example from the Median Tectonic Line, Japan. Journal of Structural Geology 28, 220–235.

Jeppson, T.N., Bradbury, K.K., Evans, J.P., 2010. Geophysical properties within the San Andreas fault zone at the San Andreas fault observatory at depth (SAFOD), and their relationships to rock properties and fault zone structure. Journal of Geophysical Research. doi:10.1029/2010JB007563 in press.

Lachenbruch, A.H., Sass, J.H., 1980. Heat flow and energetic of the San Andreas fault zone. Journal of Geophysical Research 85, 6185–6223.

Mares, V.M., Kronenberg, A.K., 1993. Experimental deformation of muscovite. Journal of Structural Geology 15, 1061–1075.

Mittempergher, S., Di Toro, G., Gratier, J., Hadizadeh, J., Smith, S.A., Desbois, G., Spiess, R., 2009. Evidences of transient increase of fluid pressure in isolated patches of the active San Andreas Fault in SAFOD phase 3 cores. Eos Transactions of the American Geophysical Union 90 (52) Fall Meeting Supplement, Abstract T52B–04.

Moore, D.E., Rymer, M.J., 2007. Talc-bearing serpentinite and the creeping section of the San Andreas fault. Nature 448, 795–797.

Morrow, C., Solum, J., Tembe, S., Lockner, D., Wong, T.F., 2007. Using drill cutting separates to estimate the strength of narrow shear zones at SAFOD. Geophysical Research Letters 34 (L11301). doi:10.1029/2007GL029665.

Mount, V.S., Suppe, J., 1987. State of stress near the San Andreas fault: implications for wrench tectonics. Geology 15, 1143–1146.

Niemeijer, A.R., Spiers, C.J., 2005. Influence of phyllosilicates on fault strength in the brittle-ductile transition: insights from rock analogue experiments. In: Bruhn, D., Burlini, L. (Eds.), High Strain Zones: Structure and Physical Properties. Geological Society of London, Special Publication, vol. 245, pp. 303–327.

SAFOD, 2010. The core atlas (version 4) available from. http://www.earthscope.org/es_doc/data/safod/Core%20Photo%20Atlas%20v4.pdf.

Saffer, D.M., Frye, K.M., Marone, C., Mair, K., 2001. Laboratory results indicating complex and potentially unstable frictional behavior of smectite clay. Geophysical Research Letters 28, 12. doi:10.1029/2001GL012869.

Saffer, D.M., Marone, C., 2003. Comparison of smectite- and illite-rich gouge frictional properties: application to the updip limit of the seismogenic zone along subduction megathrusts. Earth and Planetary Science Letters 215, 219–235.

Sass, J., Williams, C., Lachenbruch, A., Galanis, S., Grubb, F., 1997. Thermal regime of the San Andreas fault near Parkfield, California. Journal of Geophysical Research 102 (B12). doi:10.1029/JB102iB12p27575.

Schleicher, A.M., van der Pluijm, B.A., Warr, L.N., 2006. Origin and significance of clay-coated fractures in mudrock fragments of the SAFOD borehole (Parkfield, California). Geophysical Research Letters 33 (L16313–L16317). doi:10.1029/2006GL026505.

Schleicher, A.M., Tourscher, S.N., van der Pluijm, B.A., Warr, L.N., 2009a. Constraints on mineralization, fluid-rock interaction, and mass transfer during faulting at 2–3 km depth from the SAFOD drill hole. Journal of Geophysical Research 114. doi:10.1029/2008JB006092.

Schleicher, A.M., Warr, L.N., van der Pluijm, B.A., 2009b. On the origin of mixedlayered clay minerals from the San Andreas Fault at 2.5–3 km vertical depth (SAFOD drillhole at Parkfield, California). Contributions to Mineralogy and Petrology 157, 173–187. doi:10.1007/s00410-008-0328-7.

Schleicher, A.M., van der Pluijm, B.A., Warr, L.N., 2010. Nanocoatings of clay and creep of the San Andreas fault at Parkfield, California. Geology 38, 667–670. doi:10.1130/G31091.1.

Scholz, C.H., 2000. Evidence for a strong San Andreas fault. Geology 28, 163–166.

Sills, D.W., Chester, J.S., Chester, F.M., 2009. Shape-preferred orientation of porphyroclasts in the active gouge zones of the San Andreas Fault at SAFOD. Eos Transactions AGU 90 (52) Fall Meeting Supplement, abstract T43A-2057.

Solum, J.G., Hickman, S.H., Lockner, D.A., Moore, D.E., van der Pluijm, B.A., Schleicher, A.M., Evans, J.P., 2006. Mineralogical characterization of protolith and fault rocks from the SAFOD Main Hole. Geophysical Research Letters 33 (L21314–L21318). doi:10.1029/2006GL027285.

Tembe, S., Lockner, D.A., Solum, J.G., Morrow, C.A., Wong, T.-F., Moore, D.E., 2006. Frictional strength of cuttings and core from SAFOD drillhole phases 1 and 2. Geophysical Research Letters 33. doi:10.1029/2006GL027626.

Titus, S.J., DeMets, C., Tikoff, B., 2006. Thirty-five-year creep rates for the creeping segment of the San Andreas Fault and the effects of the 2004 Parkfield earthquake: constraints from alignement arrays, continuous global positioning system, and creepmeter. Bulletin of the Seismological Society of America 96, S250–S268. doi:10.1785/0120050811.

Van Breemen, N., Buurman, P., 2002. Soil Formation. Kluwer Academic Publishers, Dordrecht, Netherlands, p. 404.

Wakabayashi, J., 1999. The Franciscan Complex, San Francisco Bay area: a record of subduction complex processes. In: Wagner, D.L., Graham, S.A. (Eds.), Geologic Field Trips in Northern California, vol. 119. California Division of Mines and Geology, Special Publication, pp. 1–21.

Wang, C.-Y., 1984. On the constitution of the San Andreas fault zone in Central California. Journal of Geophysical Research 89, 5858–5866.

Wiersberg, T., Erzinger, J., 2008. On the origin and spatial distribution of gas at seismogenic depths of the San Andreas Fault from drill mud gas analysis. Applied Geochemistry 23, 1675–1690.

Williams, C.F., D'Alessio, M.A., Grubb, F.V., Galanis, S.P., 2005. Heat flow in the SAFOD main hole. Eos Transactions of the American Geophysical Union 86 (52) Fall Meeting Supplement, Abstract T23E-07.

Wintsch, R.P., Christoffersen, R., Kronenberg, A.K., 1995. Fluid-rock reaction weakening of fault zones. Journal of Geophysical Research 100, 13021–13032.

Zoback, M.D., 2000. Strength of the San Andreas. Nature 405, 31–32.

Zoback, M.D., Hickman, S.H., 2005. Preliminary observations of stress and fluid pressure in and near the San Andreas Fault at depth in the SAFOD boreholes. Eos: Transactions of the American Geophysical Union 86 (52) Fall Meeting Supplement, Abstract T21A-0438.

Zoback, M.D., Hickman, S.H., Ellsworth, B., 2010. Scientific drilling into the San Andreas fault zone. Eos: Transactions of the American Geophysical Union 91 (22), 197–199.

Zoback, M.D., Hickman, S.H., Ellsworth, W., Kirschner, D., Pennell, N.B., Chery, J., Sobolev, S., 2007. Preliminary Results from SAFOD Phase 3: implications for the state of stress and shear localization in and near the San Andreas Fault at depth in central California. Eos Transactions of the American Geophysical Union 88 (52) Fall Meet. Suppl. Abstract T13 G-03.

Zoback, M.D., Zoback, M.L., Mount, V.S., Suppe, J., Eaton, J.P., Healy, J.H., Oppenheimer, D., Reasenberg, P., Jones, L., Rayleigh, C.B., Wong, I.G., Scotti, O., Wentworth, C., 1987. New evidence on the state of stress of the San Andreas fault system. Science 238, 1105–1111.